Emergence of Luttinger liquid behavior of a superclimbing dislocation

M. Yarmolinsky and A. B. Kuklov

Department of Engineering and Physics, College of Staten Island and the Graduate Center, CUNY, Staten Island, New York 10314, USA

(Received 6 December 2016; revised manuscript received 5 June 2017; published 7 July 2017)

A generic edge dislocation with superfluid core in solid ^{4}He represents a non-Luttinger liquid according to the elementary scaling dimensional analysis because its compressibility is *giant*, that is, it diverges as square of the dislocation length. Monte Carlo simulations, however, reveal that such a dislocation develops finite compressibility as temperature is lowered. Furthermore, for certain parameters the dislocation can undergo a transition into insulating state regardless of the filling factor. External *macroscopically* small bias by chemical potential can restore the giant compressibility. Experimental verifications of these features are proposed in connection with the ongoing efforts to understand the superflow-through-solid as well as the syringe effects in solid ^{4}He.

DOI: 10.1103/PhysRevB.96.024505

I. INTRODUCTION

Emergence [1] is the topic drawing a lot of attention for the last 50 years, with the most prominent examples being the charge fractionalization in fractional quantum Hall effect [2] and dynamical enlargement of the underlying symmetry at the point of continuous phase transitions [3].

Luttinger liquid (LL) is the universal description for one-dimensional (1D) conducting quantum systems. Both fermionic and bosonic quantum wires are generically described by the harmonic model of collective soundlike excitations [4]. Essentially the same approach applies to spin $S = \frac{1}{2}$ chains (see Ref. [5]). The concept of LL turns out to be relevant to solid ^{4}He too. As found in *ab initio* simulations [6], screw dislocation with Burgers vector along the high-symmetry axis possesses superfluid core. This 1D topological structural defect is essentially the bosonic LL. There is, however, a significant difference between a dislocation with superfluid core and a conducting wire. Dislocation is a dynamical string able to change its shape and to move within crystal. In quantum crystals, the string dynamics must be treated quantum mechanically. This raises a plethora of questions traditionally more relevant to high-energy physics. One key question is about how the dislocation dynamics interacts with its core superfluidity.

This question is especially relevant in connection with the superflow through solid ^{4}He observed first in the UMASS group [7] and then confirmed by other groups [8–10]. There is one strikingly unexpected feature serendipitously observed in the UMASS group [7]: during the superflow events the solid exhibits the response on external chemical potential, practically, the same way as liquid does, i.e., it absorbs or expels a macroscopic fraction of atoms. This effect, which was called *giant isochoric compressibility* (or *syringe* effect) in Ref. [11], represents a mechanism of crystal growth from inside out. Both effects are now at the focus of the experimental and theoretical efforts in the field of superfluidity and quantum crystals.

It is important to realize that a dislocation with superfluid core in a crystal represents a supersolid state of matter, that is, the coexistence of superfluidity with crystalline symmetry both formed by the same atoms (see the discussion about various types of supersolidity in [12]). Indeed, despite breaking the hexagonal close packing (hcp) symmetry of the ideal crystal, the dislocation [6] aligned with the high-symmetry axis preserves perfect periodicity of the crystal along this axis. It also retains the C_6 symmetry of rotations with respect to the dislocation core. This supersolid, however, is quite different from the supersolid phase of ideal crystal confining a condensate of zero point vacancies contemplated by Andreev and Lifshitz [13]. As has been shown in Ref. [14], vacancies in solid ^{4}He attract each other and, therefore, cannot form stable Bose-Einstein condensate at zero temperature (T) in ideal crystal; they tend to agglomerate into dislocation loops. The situation is completely different in vicinity of topological defects where local strain is topologically protected and, thus, induces stable low-D superfluidity [15] along some dislocations [6,11] and some grain boundaries [16].

There is a new property emerging due to the core superfluidity: such a dislocation can perform nonconservative motion, that is, climb [17,18]. In Ref. [11] this effect has been called *superclimb*, climb supported by superflow along the dislocation core. A pure screw dislocation cannot perform superclimb. However, deviations of the core orientation from the direction of the Burgers vector transform screw dislocation into *edge* dislocation (see in, e.g., [17–19]). In this case, the core retaining its superfluidity can perform superclimb. In this case, as discussed in [11], spectrum of excitations is no more linear in the momentum along the core. Thus, a superclimbing dislocation is not expected to be LL and should be classified as non-LL.

The superclimb has been proposed in Ref. [11] as a possible explanation for the syringe effect. In other words, edge dislocations with superfluid core can supply matter into (from) the solid by building (dissolving) incomplete atomic planes. The syringe effect has also been seen by the University of Alberta group [8], and very recently confirmed in its most conspicuous form in Ref. [9]. At the moment, however, there is no direct proof that the syringe effect is due to the superclimb of dislocations. Thus, it is important to find features of the dislocation scenario which can be tested experimentally.

The main prediction about superclimb put forward in [11] is about edge dislocation aligned with single Peierls potential (see [17–19]) valley. Such a dislocation becomes self-trapped by the potential at $T = 0$. Thus, if all the edge dislocations with superfluid core were self-trapped, the syringe effect should vanish. However, a generic dislocation network in real crystals

is mostly disordered. Thus, there should be dislocations which are not aligned with the Peierls valleys. Accordingly, such dislocations are characterized by finite density of jogs (see [18]) which form a quantum fluid supporting superclimb even at $T = 0$ [20].

Here, we revise the conjecture [20] based on the standard analysis of the relevance of Peierls potential. Our main result is that, as temperature decreases, superclimb of a generic edge dislocation (that is, not aligned with one Peierls valley) with superfluid core must be suppressed. This reinstates the linear excitation spectrum and, consequently, the LL character of the superfluidity along the core. Below we will, first, briefly review the superclimb effect. Then, we will discuss the results of large-scale simulations of the model of the superclimbing dislocation and will present the evidence for the emergence of the LL behavior as well as its destruction by bias. Finally, we will discuss the features to look for in experiment in order to test the dislocation scenario for the superflow and the syringe effects.

II. SUPERCLIMB AND THE GIANT ISOCHORIC COMPRESSIBILITY

Dislocations are most typical 1D structural topological defects in crystals (see Refs. [17–19]). These are characterized by position and shape of its core as well as by the Burgers vector which is determined by the crystalline symmetry. Symmetry relevant to solid ^{4}He is the hexagonal close packed (hcp) structure (see Refs. [17,18]). Its highest-symmetry axis is called C axis and it has C_6 symmetry. It is perpendicular to the *basal* planes which are triangular two-dimensional (2D) lattices. The hcp structure has two basic types of dislocations: with Burgers vector belonging to the basal plane and along the C axis.

Ab initio simulations of dislocations with the Burgers vector along the C axis have found that these dislocations in solid ^{4}He have superfluid core. Superfluidity of the screw dislocation (with the core and the Burgers vector being along the C axis) has been reported in Ref. [6]. Similarly, the superfluid core has been found in the edge dislocation with the Burgers along C axis, and it has been reported in Ref. [11].

There is a significant difference between the two dislocations: while the edge dislocation can perform superclimb [11] as a linear response on chemical potential μ, the screw one cannot. Thus, a dislocation with superfluid core meandering through solid should consist of edge and screw segments. A possible resulting network of such dislocations is shown in Fig. 1. One superclimbing segment of length L of the network is schematically shown in Fig. 2. The matter can be fed into the dislocation from its ends contacting other dislocations with superfluid core or a reservoir with superfluid. As a result, extra matter is supplied to or taken away from an incomplete basal plane of atoms. Accordingly, the dislocation core (depicted by the ragged solid line in Fig. 2) can shift (up or down).

It is important to discuss the role of external bias by chemical potential μ. A small change of chemical potential imposed on a liquid results in a small change of the liquid density ρ. The corresponding dependence ρ versus μ is smooth with the finite slope $d\rho/d\mu$ which is the isochoric compressibility. In a standard LL this quantity is independent of the length L. The situation is very different in the case

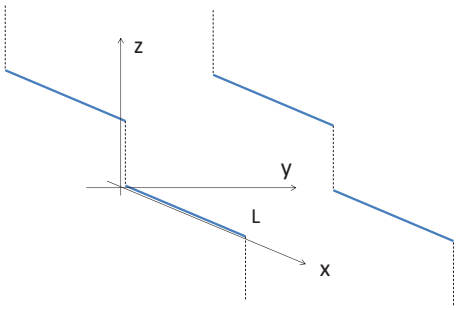

FIG. 1. A forest of dislocations with Burgers along the hcp axis (Z axis) containing edge superclimbing segments (thick solid lines aligned with X axis) and pure screw ones (dashed lines along Z axis). Superclimb of the edge segments occurs in the XY planes along the Y axis.

of the superclimbing dislocation: imposing a finite bias by μ does not produce any significant change of the superfluid density inside the core. Instead, the core shifts (up or down as sketched in Fig. 2) by the amount exactly determined by the number of atoms N traveled along the core to build an incomplete atomic plane (shown by dashed lines in Fig. 2). In this case, the isochoric compressibility $\kappa = L^{-1}dN/d\mu$ becomes "giant" [11], that is, $\kappa \propto L^2$. For consistency, this feature reported in Ref. [11] will be explained in detail below.

A superclimbing dislocation [11] is modeled as an elastic string of length L. In the absence of the Peierls potential it is represented by the action in imaginary time τ:

$$S = \int_0^\beta d\tau \int_0^L dx \Big[-i(y + n_0)\partial_\tau \phi + \frac{\rho_0}{2}(\partial_x \phi)^2 + \frac{\kappa_0}{2}(\partial_\tau \phi)^2 + \frac{G}{2}(\partial_x y)^2 - \mu y \Big] \quad (1)$$

(in units $\hbar = 1$, $K_B = 1$), where all distances (here and below) are measured in terms of a typical interatomic distance. This action describes the displacement $y = y(x,\tau)$ of the dislocation, depicted in Fig. 2, from its equilibrium position $y = 0$. As mentioned above, $y(x,\tau)$ determines the total amount of atoms ΔN entered (exited) through the dislocation

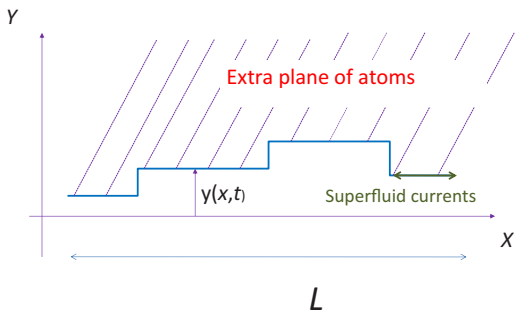

FIG. 2. Superclimbing dislocation (solid ragged line) as indicated by the edge of an incomplete atomic basal plane (dashed lines). The double arrow shows the directions of the superflow along the core.

ends. This implies

$$\Delta N(\tau) = \int_0^L dx\, y(x,\tau). \tag{2}$$

The quantity $\phi = \phi(x,\tau)$ represents the superfluid phase defined along the superfluid core. Here, $\beta = 1/T$, ρ_0 and κ_0 are bare superfluid stiffness and superfluid compressibility, respectively; G stands for the effective tension of the dislocation ($\sim$ shear modulus); and the last term accounts for the bias by chemical potential μ. The quantity n_0 describes average (linear) density of bosons. We consider the limits $\omega \to 0$, $q \to 0$. Thus, $\sim(\partial_\tau y)^2$ representing kinetic energy of the dislocation is omitted from Eq. (1). To exclude the zero mode where the uniform shift of the dislocation as a whole costs no energy, the boundary condition $y(x=0,\tau) = y(x = L,\tau) = 0$ is used. This condition is, in particular, relevant to the type of a network shown in Fig. 1, where the meeting region of the screw and edge segments plays the role of the pinning point for superclimb because the screw segment cannot perform superclimb for arbitrary small bias μ.

If there were no climb (that is, $y = 0$), the model (1) would represent the standard LL characterized by the linear excitation spectrum $\omega = \sqrt{\rho_0/\kappa_0}q$ with respect to the wave vector q along the dislocation [4]. The situation changes dramatically in the presence of the climb: The imaginary term in Eq. (1) (the Berry term) counts how many particles passed through the dislocation core and ended up in an extra row of atoms advancing dislocation by y. This effect changes the spectrum from linear to parabolic. Indeed, variational equations $\delta S/\delta\phi = 0$, $\delta S/\delta y = 0$ following from the action (1) give $\partial_\tau^2 y - G\rho_0\partial_x^4 y = 0$ in the long-wave limit. In real time $t = i\tau$, this corresponds to the parabolic spectrum $\omega = \sqrt{G\rho_0}q^2$ as $q \to 0$. Thus, the action (1) describes a non-LL.

A. Giant isochoric compressibility

If the superfluid stiffness ρ_0 in Eq. (1) is finite and the dislocation ends are connected to a superfluid reservoir, biasing by finite μ will result in the dislocation bowing by $y \sim L^2\mu/G$. More accurately, the solution minimizing the action (1) is $y(x) = x(L-x)\mu/2G$ which corresponds to $DN = \int dx\, y = \mu L^3/12G$. Accordingly, the compressibility

$$\kappa = \frac{d\Delta N}{Ld\mu} \to \kappa_g = \frac{L^2}{12G} \propto L^2 \tag{3}$$

becomes *giant* as opposed to $\kappa = \kappa_0 \propto L^0$ in the absence of the variable y in Eq. (1).

It is important to realize that a sample of bulk solid ^{4}He permeated by a uniform network of such dislocations must show a finite three-dimensional (3D) compressibility κ_{3D}, very similar to that of a 3D liquid. In other words, κ_{3D} is *independent* of the dislocation density (as long as this density is small in units of interatomic distance). Let us demonstrate this using a simplistic example of a network consisting of rectangular parallelepipeds with edges of typical lengths L_x, L_y, L_z. One element of such a network is sketched in Fig. 3. Let us presume that the edges of length L_x along X direction represent edge (superclimbing) segments of dislocations with superfluid core. The distance L_y characterizes a typical separation between such segments. The distance L_z characterizes a typical length of the screw (nonsuperclimbing) segments (as sketched in Fig. 1).

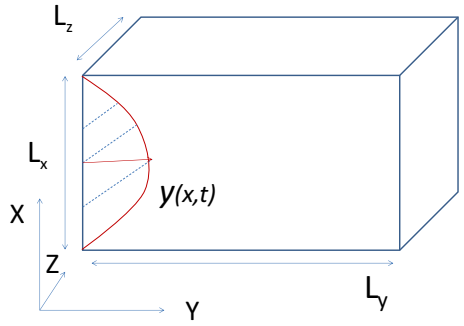

FIG. 3. One block of the dislocation network built by dislocations with superfluid core. Superclimbing dislocations, the edges along X direction, bend in response to the bias by chemical potential μ, as shown by the bulging line. The added matter is depicted by dashed lines (only one edge is shown to bulge).

Biasing the network by μ results in bowing the edge segments by $y \sim \mu L_x^2/G$. This implies an additional amount of atoms $\Delta N \sim yL_x \sim \mu L_x^3/G$ per each element. Consequently, the bulk density δn changes as

$$\delta n \approx \frac{\Delta N}{L_x L_y L_z} \sim \frac{L_x^2}{L_y L_z}\frac{\mu}{G}. \tag{4}$$

Thus, $\kappa_{3D} = \delta n/\delta\mu$ depends only on the *ratio* of the free segment lengths. In other words, uniformly increasing all lengths L_x, L_y, L_z by the same factor, say, 2, does not change the above result (4), while decreasing the dislocation density by the factor of 4.

It is important to note that it is enough to apply μ just at a point contact with the network to introduce the density change (4). This is the same outcome as if μ were applied to a fluid. In contrast, applying μ (at any point) to an ideal solid (without dislocations) does not cause any detectable change of its overall density. In this sense, the response (4) of the real solid should be viewed as *giant*. Clearly, if the superclimbing segments are to evolve into LLs and, thus, to lose their giant compressibility (3), the response (4) of the solid (the syringe effect) will vanish, that is $\kappa_{3D} = 0$.

As a matter of fact, the response on μ is not completely that of a liquid, where in equilibrium pressure variation distributes uniformly over the whole liquid, in accordance with the Pascal law. Viewing this property from the perspective of chemical potential, a pressure change ΔP in a liquid in response on applying a change μ of chemical potential must be exactly equal to μ. This constitutes a maximum possible syringe effect. In a solid permeated by the dislocation network, while the compressibility κ_{3D} is finite as described above, the resulting pressure change $\Delta P \neq \mu$.

B. Collective effects

As described in Ref. [21], presence of an ensemble of dislocations modifies the isochoric compressibility. The main effect comes from the overall compression of the solid as extra matter ΔN enters (exits) it. Referring to one element of the network, Fig. 3, the energy of the bowing with account for the compression energy $\sim K_{el}L_xL_yL_z\Delta N^2/2N^2$, where

$N \sim L_x L_y L_z$ stands for the total number of atoms in the volume of one cell and K_{el} stands for the compression modulus, can be written as

$$E \sim \frac{Gy^2}{2L_x} + \frac{K_{el}\Delta N^2}{2L_x L_y L_z} - \mu y L_x, \ \Delta N \sim y L_x. \tag{5}$$

The equilibrium value for y follows from the minimization of E. This gives the fractional density change $\Delta N/N$ and the corresponding pressure change in the solid as $\Delta P \sim K_{el}\Delta N/N$:

$$\Delta P \approx \frac{K_{el}}{G L_y L_z L_x^{-2} + K_{el}}\mu. \tag{6}$$

If the shear modulus were zero, that is, $G = 0$, the pressure change would be exactly that of a liquid. This limit can also be reached in the case of a highly asymmetric network with $L_x \gg \sqrt{L_y L_z}$.

C. Compressibility and dislocation excitation spectrum

Concluding this section, we emphasize that the renormalized compressibility κ and the superfluid stiffness ρ_s both determine the spectrum of excitations of the dislocation as $\omega = \sqrt{\rho_s/\kappa}\, q$, with q being a wave vector along the dislocation. In the case of the screw dislocation, both κ and ρ_s are finite (that is independent of q) and, thus, the spectrum is soundlike. This implies the LL behavior. In the case of the superclimbing edge dislocation, κ depends on the wavelength as $\kappa \sim 1/q^2$ (up to the dislocation length $\kappa \sim L^2$), and this leads to the parabolic spectrum $\omega \propto q^2$ as mentioned previously. This is why superclimbing dislocation represents non-LL. If superclimb is suppressed by, say, Peierls potential or impurities, κ becomes finite and the linear spectrum is recovered, that is, the LL is restored. This effect spontaneously occurring as $T \to 0$ will be reported in the following section.

III. SUPERCLIMB BEYOND THE GAUSSIAN APPROXIMATION

The discussion in the previous section was based on the Gaussian approximation, that is, it ignored the compact nature of the phase ϕ in the action (1). In other words, the possibility of instantons in the $D = 1 + 1$ space-time was not taken into account. Furthermore, there is no term corresponding to the Peierls potential in the action (1). In its simplest form $\sim\int d\tau \int dx \cos(2\pi y)$, this term takes into account the periodic potential imposed by the lattice and seen by the dislocation during its climbs. As discussed in [11], this term suppresses the superclimb at $T = 0$, if the equilibrium configuration corresponds to $y(x) = 0$ (or any other minimum $y = n$, $n = \pm 1, \pm 2, \ldots$). Then, the compressibility becomes finite (with respect to $L \to \infty$), and the spectrum of excitations becomes soundlike. In other words, the LL behavior of the dislocation core superflow is restored as long as the dislocation is aligned with one of the Peierls valleys.

Generically, however, dislocations form a network containing dislocations not aligned with Peierls valleys. More specifically, the dislocation end at $x = 0$ may be pinned at, say $y(x = 0,\tau) = 0$, and the other one at $y(x = L,\tau) = n$ with $n \neq 0$. This dislocation is said to be tilted in the Peierls potential. Accordingly, it has n jogs even at $T = 0$. Such geometrical jogs can be taken into account by shifting $y \to y + nx/L$ in the action and accordingly in the Peierls energy $\int dx \cos(2\pi y/a) \to \int dx \cos(2\pi y + 2\pi n x/L)$, where now the boundary condition becomes $y(0,\tau) = y(L,\tau) = 0$.

The standard approach to treating the cos(...) potential (see, e.g., in Ref. [19]) is based on the assumption that the term $2\pi n x/L$ washes out the potential. As suggested in [20], this implies that the geometrical jogs form quantum fluid of jogs which protect the superclimb from suppression at $T = 0$. In other words, the compressibility κ should remain giant as given by Eq. (3) at $T = 0$. Accordingly, the excitation spectrum remains quadratic in q, that is, the superfluidity along the core is of the non-LL type. This argument, however, has not been verified numerically.

Here, we analyze a tilted superclimbing dislocation beyond the Gaussian approximation by Monte Carlo simulations of the model [11] with no Peierls potential. The main purpose of this is to understand the role of compactness of the phase ϕ in the action (1). As will be shown below, this property turns out to be crucial as $T \to 0$ leading to the restoration of the LL character of the core superfluidity by suppressing the superclimb. At this point, we also mention that the external bias μ in the action (1) can destroy the LL and restore the superclimb as long as μ exceeds a threshold which is *macroscopically* small with respect to L. This effect will be discussed later in Sec. IV.

A. Dual representation

Here, we will go beyond the Gaussian approximation in (1) and take into account the compact nature of the phase ϕ by allowing vortices (instantons) to exist in the space-time (x,τ). This, in particular, can be achieved by discretizing the space-time so that $\int d\tau \int dx \ldots$ transforms into a sum over the space-time lattice. The discretization of space is justified by the presence of the crystalline 3D lattice introducing the natural increment $\Delta x \approx a$ determined by a typical interatomic distance a along the dislocation core. Then, the continuous derivative becomes discrete: $\partial_x\phi(x,\tau) \to \nabla_x\phi = \phi(x + 1,\tau) - \phi(x,\tau)$ where we use a as the unit of x.

The continuous time derivative transforms as $\partial_\tau\phi(x,\tau) \to \nabla_\tau\phi = [\phi(x,\tau + \Delta\tau) - \phi(x,\tau)]/\Delta\tau$, where $\Delta\tau$ is the unit of the time discretization $\Delta\tau = \beta/N_\tau \to 0$, with N_τ being the number of time slices in the time interval $(0,\beta)$. Then, the compactness of ϕ is taken into account by using the Villain transformation $\vec{\nabla}\phi \to \vec{\nabla}\phi + 2\pi\vec{m}$ [22], where the vector sign refers to the space-time directions and $\vec{m} = (m_\tau, m_x)$ stands for integer variables defined on (and oriented along) bonds between neighboring sites of the space-time lattice. This approach allows treating ϕ as a noncompact Gaussian variable, on the expense of introducing the bond variables $\vec{m}$.

The thermodynamics of the model (1) (with the substitute $\vec{\nabla}\phi \to \vec{\nabla}\phi + 2\pi\vec{m}$) can be accounted for within the partition function

$$Z = \sum_{\{\vec{m}\}} \int D\phi \int Dy \exp(-S), \tag{7}$$

where the action (1) takes the form

$$S=\sum_{(\tau,x)}\Big[-i(y+n_0)\nabla_\tau(\phi+2\pi m_\tau)+\frac{\rho_0}{2}(\nabla_x\phi+2\pi m_x)^2 +\frac{\kappa_0}{2}(\nabla_\tau\phi+2\pi m_x)^2+\frac{G}{2}(\partial_x y)^2-\mu y\Big]. \quad (8)$$

It is convenient to use Poisson identity $\sum_m f(m)\equiv\sum_n\int dm f(m)\exp(2\pi imn)$ at each bond along the line of the derivation of the J-current model [23]. Then, the integrations over $\vec{m},\phi,y$ can be carried over exactly. This transforms Eq. (7) into

$$Z=\sum_{\{\vec{J}=(J_x,J_\tau)\}}\exp(-S_J), \quad (9)$$

where the action S_J (in the long-wave limit) is

$$S_J=\sum_{b_{ij}}\Big[\frac{J_x^2}{2\tilde{\rho}_0}+\frac{\tilde{G}}{2}(\nabla_x J_\tau)^2-\tilde{\mu}J_\tau\Big], \quad (10)$$

with $\tilde{G}=G\Delta\tau$, $\tilde{\mu}=\mu\Delta\tau$, and $\tilde{\rho}_0=1/[2\ln(2/\rho_0\Delta\tau)]$ (in the limit $\Delta\tau\to 0$ [22]). The integer bond oriented currents $\vec{J}$ (that is, $|\vec{J}|=0,1,2,...$) between neighboring sites satisfy the Kirchhoff's conservation rule, and the summation is performed over all bonds b_{ij} between all pairs of neighboring sites i and j. It should be kept in mind that $\vec{J}=(J_x,J_\tau)$ is oriented either along a spatial or a temporal bond. In other words, if b_{ij} is a bond along the X direction, the current along this bond has zero temporal component, $J_\tau=0$. Similarly, $J_x=0$ on a bond oriented along the imaginary-time axis.

The action (10) is a dual representation of the models (7) and (8). The boundary condition for y is transformed into $J_\tau(x=0,\tau)=J_\tau(x=L,\tau)=0$ in addition to the periodic boundary condition along time: $\vec{J}(x,\tau+\beta)=\vec{J}(x,\tau)$, $\vec{J}(x+L,\tau)=\vec{J}(x,\tau)$.

The striking difference between the action (10) and the standard one of the J-current model [23] describing LL is the absence of the term $\sim J_\tau^2$. As we will show below, such a term will be *emerging* as $T\to 0$ and $\mu\to 0$.

B. Linear response

The linear response of the system is described in terms of the renormalized stiffness along space [24]

$$\rho_s=\frac{L}{N_\tau}\langle W_x^2\rangle,\quad W_x=\frac{1}{L}\sum_{\vec{b}_{ij}}J_x, \quad (11)$$

and along time, which is the renormalized compressibility:

$$\kappa=-\frac{N_\tau}{L}\frac{\partial^2\ln Z}{\partial\mu^2}=\frac{N_\tau}{L}\big[\langle W_\tau^2\rangle-\langle W_\tau\rangle^2\big]. \quad (12)$$

The quantities W_x, $W_\tau=N_\tau^{-1}\sum_{\vec{b}_{ij}}J_\tau$ are integers and have the geometrical meaning of windings of the lines formed by the J currents. We have also calculated

$$\kappa_1=\frac{\langle N\rangle}{L\mu}=\frac{\langle W_\tau\rangle}{L\mu} \quad (13)$$

characterized by the total number of atoms $\langle N\rangle=\langle W_\tau\rangle/N_\tau$ injected into the solid due to the superclimb. Both quantities κ and κ_1 coincide with each other as $\mu\to 0$. In general, these are related by the exact formula $\kappa=d(\mu\kappa_1)/d\mu$. Simulations have been performed by the Worm algorithm [25].

C. Emergence of the LL behavior

Here, we will present the evidence that, as the dislocation length L and the inverse temperature β both increase as $\beta\propto L\to\infty$, the compressibility κ crosses over from being "giant" [Eq. (3)] to $\kappa=\kappa_{\rm eff}$ saturating to a finite value in this limit. This implies the reconstruction of the excitation spectrum from parabolic to linear. In other words, the superclimb is being suppressed and the LL behavior emerges. We will also show that the phase diagram of the systems (9) and (10) in the plane (ρ_0,G), $\mu=0$, features two phases: LL and insulator (where both ρ_s and κ vanish).

Strictly speaking, all results of simulations of the models (9) and (10) should be considered in the limit $N_\tau\to\infty$ in order to achieve the continuous time result. Practically, N_τ should be taken as large as needed to stop simulated quantities being dependent on N_τ for a given value of β. The result of this procedure is shown in Fig. 4.

The compressibility deviates from its giant value [Eq. (3)] as temperature decreases and asymptotically approaches some value which is more than one order of magnitude smaller than κ_g [Eq. (3)] for a given size L. The question is how the asymptotic value of κ depends on L. The result of simulations for several sizes of L are presented in Fig. 5. As can be seen, the asymptotic values of κ (in the limit $T\to 0$) are independent of L for large enough L. The asymptotic independence of κ on L is seen much more clearly in Fig. 6 where $T^{-1}=\beta$ is scaled as $\sim L\to\infty$.

A comment is in order about the procedure used to collect the data in Figs. 5 and 6 and from now on. We have checked that, while changing specific values, the qualitative behavior of κ remains the same for a fixed value of N_τ for given L without formally achieving the quantum limit of continuous

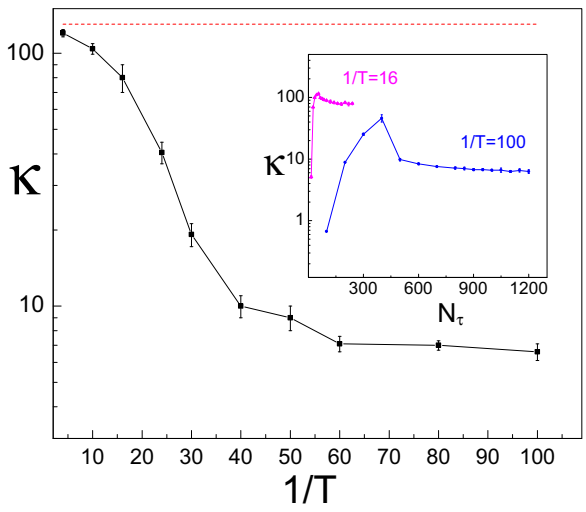

FIG. 4. κ [Eq. (12)] vs $\beta=T^{-1}$ for $L=60$, $G=2.3$, $\rho_0=4$, $\mu=0$. Inset: κ vs the number of time slices N_τ for two temperatures (shown close to each curve). The horizontal dashed line corresponds to the value of the "giant" compressibility [Eq. (3)].

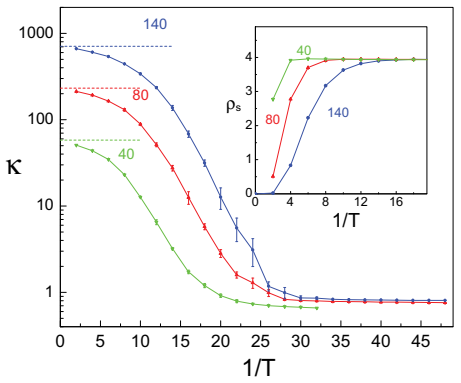

FIG. 5. κ vs $\beta = T^{-1}$ for the lengths $L = 40,80,140$ (shown close to each curve). The horizontal dashed lines are the corresponding values of the giant compressibility [Eq. (3)]. Inset: superfluid stiffness vs T^{-1} for the same sizes. The model parameters are $\rho_0 = 4$, $G = 2.3$, $\mu = 0$ in Eq. (10).

time. Thus, the data in Fig. 5 and below are presented for $T = 1/N_\tau$, that is, for the choice $\Delta\tau = 1$ (and $\tilde{G} = G$, $\tilde{\rho}_0 = \rho_0$, $\tilde{\mu} = \mu$).

The dependence κ vs T is characterized by some typical temperature $T = T_L$ and the range Δ_L below which κ becomes significantly suppressed. In order to evaluate T_L and the width Δ_L, we have found the best fit of κ vs $1/T$ using T_L and Δ_L as the fit parameter in the fit function taken as $\ln(\kappa) = A - B\tanh[\Delta_L(T^{-1} - T_L^{-1})]$, with A and B chosen from the limiting values of κ at the highest and lowest T for each L. This function has produced fits which are acceptable within the statistical errors of the data for all curves. We have found that the crossover temperature $T_L \sim 1/\ln L$ and its width $\Delta_L \sim 1/\ln L$. More specifically, for $G = 2.3$, $\rho_0 = 4$, $\mu = 0$, the dependencies on L are $T_L^{-1} = a\ln L + b$, with $a = 5.02$, $b = -6.27$ and $\Delta_L^{-1} = a'\ln L + b'$ with $a' = 1.53$, $b' = 0.09$. These dependencies are shown in Fig. 7.

The question is how the emerged compressibility in the limit $L = \infty$ depends on the parameters of the model (10). Figure 6 presents results of simulations for various values of G. The

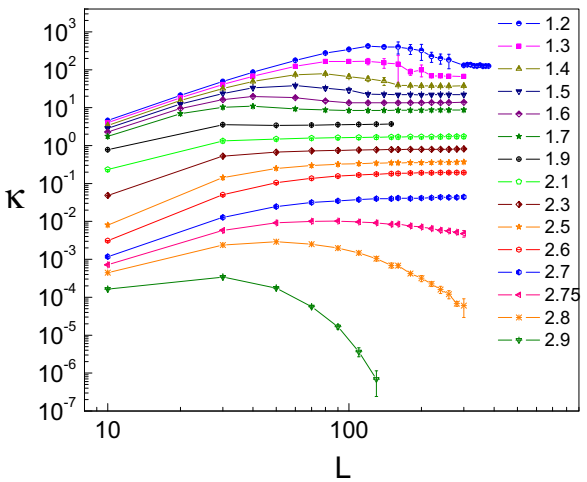

FIG. 6. Compressibility κ vs $L = 1/T$ for various values of G (shown in the legend) and $\rho_0 = 4$, $\mu = 0$.

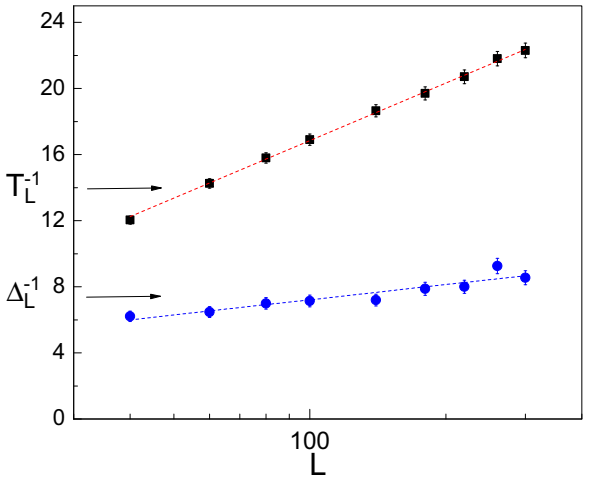

FIG. 7. The inverse crossover temperature T_L^{-1} and the width Δ_L^{-1} vs L for $G = 2.3$, $\rho_0 = 4$.

limiting value of $\kappa_{\rm eff} = \kappa$ taken from the saturated behavior at large L from Fig. 6 turns out to be $\kappa_{\rm eff} \sim 1/G^b$, $b = 7.8 \pm 0.1$ for $G < 2.6$. This dependence is shown in Fig. 8. We have tested several values of ρ_0 and did not find any dependence of the power b on it.

The effect of emergence of finite κ occurs above some length L^*(as long as $T \sim L^{-1}$). For $L < L^*$ the compressibility behaves as $\sim L^2/G$ [Eq. (3)]. For $L > L^*$ it levels off at $\sim 1/G^b$. Thus, the relation $L^{*2}/G \sim G^{-b}$ determines the crossover scale $L^* \sim G^{(1-b)/2}$ diverging in the limit $G \to 0$. Below we will discuss the deviations from the power law seen in Fig. 8 for $G \geqslant 2.6$.

D. Quantum phase transition (QPT)

If the parameter G exceeds a certain threshold G_c for a given ρ_0, there is no more saturation of κ [Eq. (12)] to a finite value in the limit $\beta \propto L \to \infty$. Instead, it flows to zero. This behavior is clearly exhibited by three lower curves in Fig. 6, corresponding to $G > 2.7$. The same tendency is seen in Fig. 8

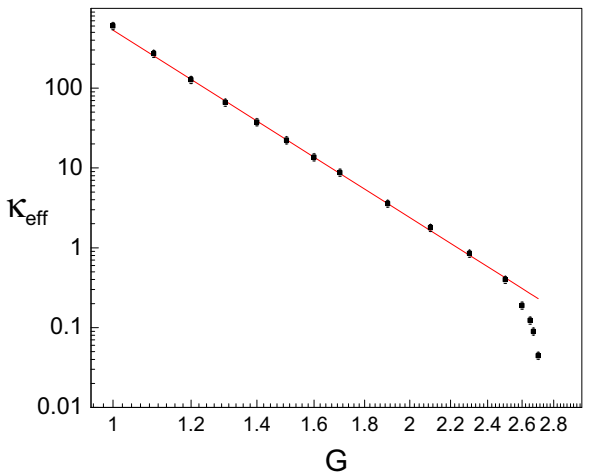

FIG. 8. The asymptotic values $\kappa_{\rm eff}$ of κ taken from Fig. 6 in the limit $L \to \infty$ for various G values.

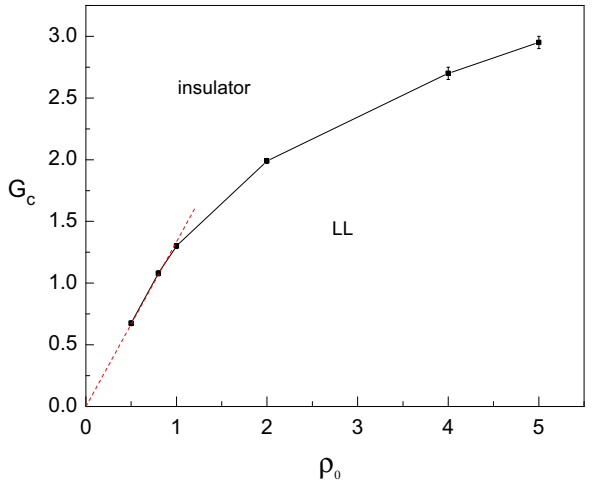

FIG. 9. The phase diagram of the models (9) and (10). Dashed straight line connects three data points with smallest ρ_0 and the origin.

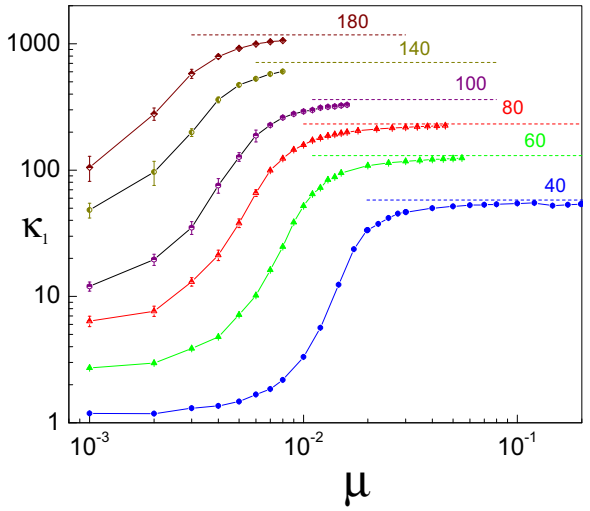

FIG. 10. κ_1 vs μ for sizes L shown close to the corresponding plot, $G = 2.3$, $\rho_0 = 4$, $T = 0.0556$, $T_H \approx 0.0435$. Dashed lines show the giant values [Eq. (3)] for the corresponding size L.

where the linear log-log dependence is violated for the same values of G (read off from Fig. 6 at the maximum L simulated). In fact, both κ and ρ_s [Eq. (11)] flow to zero for these values of G. This behavior implies insulating state of the dislocation, when both superclimb and superflow along the core cease to exist.

Phase diagram mapping the two ground-state phases of the dislocation is shown in Fig. 9. In the LL region κ [Eq. (12)] and the superfluid stiffness [Eq. (11)], both saturate to finite values in the limit $T^{-1} \sim L \to \infty$. In the region "insulator" both quantities approach zero values as $T^{-1} \sim L \to \infty$.

A presence of the transition in the models (9) and (10) is unexpected because the Kosterlitz-Thouless (KT) argument (see Ref. [19]) indicates that there should be no proliferation of the vortex pairs. Let us demonstrate this by performing duality transformation on the model (10). The Kirchhoff's constraint on the currents $\vec{\nabla}\vec{J} = 0$, where $\vec{\nabla}$ stands for discrete gradient, can be satisfied by the substitute $J_x = \nabla_\tau \Phi$, $J_\tau = -\nabla_x \Phi$, where Φ are integers defined at sites of the dual lattice [26]. Using this in Eq. (10) and utilizing the Poisson summation identity [along the same line how the action (10) was derived from the original one (1)], we obtain the lattice gas model $Z = \sum_{\{n_i\}} e^{-S_g}$, $S_g = \frac{1}{2}\sum_{\vec{r},\vec{r}'} U(\vec{r}-\vec{r}')n(\vec{r})n(\vec{r}'))$, where $n(\vec{r})$ are integers defined on the sites of the dual lattice and U is the interaction potential with Fourier components $\tilde{U} = (2\pi)^2/[\rho_0^{-1}\omega^2 + Gq^4]$ in the limits $\omega \to 0$ and $q \to 0$. The integers n describe vortices. In contrast with the standard superfluid, where vortices interact by logarithmic potential (see Ref. [19]), here the potential is much stronger than logarithm. It is also strongly asymmetric: along space it is increasing with separation between two points (x,τ) and (x',τ') as $\sim |x-x'|$ and along time as $\sim\sqrt{|\tau-\tau'|}$. Thus, according to the KT argument a vortex-antivortex pair cannot proliferate to destroy the algebraic order along the dislocation. However, in spite of this criterion, our simulations of the model (10) show that there is a transition into insulating state.

As more detailed analysis presented in the Appendix shows, the transition corresponds to the Berezinskii-Kosterlitz-Thouless (BKT) transition (see Ref. [19]) with the universal jump $2/\pi$ in the effective Luttinger parameter $K = \sqrt{\rho_s \kappa}$. It is also important to notice that the transition is insensitive to the filling factor n_0 in the model (1), simply because it cancels out from the dual representation (10).

IV. ROUGHENING INDUCED BY CHEMICAL POTENTIAL

The above results indicate that, in the absence of the bias by chemical potential μ, the models (9) and (10) have only two ground states, either insulator or Luttinger liquid marked by "insulator" and "LL" in Fig. 9, respectively. As temperature increases, the compressibility crosses over to the "giant" value (3).

The LL state corresponds to smooth dislocation (with $\kappa = \kappa_{\rm eff}$) because fluctuations of the dislocation shape $y(x,\tau)$ are strongly suppressed. This situation changes quite dramatically in the presence of finite μ in the action (10). Namely, the smooth state of the dislocation can be destroyed by the bias $\mu \neq 0$. As a result, the giant compressibility is restored. This implies the roughening transition of the dislocation: fluctuations of the dislocation shape become diverging as $\sim \ln L$ in the rough phase, where $\kappa = \kappa_g$ [Eq. 3].

Simulations of the models (9) and (10) at finite μ have revealed two regimes: (i) a crossover from smooth to rough dislocation at $T > T_H$; (ii) a jumplike behavior characterized by strong hysteresis at $T < T_H$ featuring a coexistence of the smooth and rough phases of the dislocation.

A. Smooth-rough crossover

The crossover behavior at $T > T_H$ is shown in Fig. 10. As can be seen, the width of the crossover becomes smaller for larger L. To characterize this dependence, we have measured the value $\mu_{0.5}$ of μ where κ_1 reaches $\frac{1}{2}$ of its giant value (3) for a given size L. This dependence turns out to be $\mu_{0.5} \sim L^{-c}$, $c = 1.21 \pm 0.05$, and it is shown in Fig. 11.

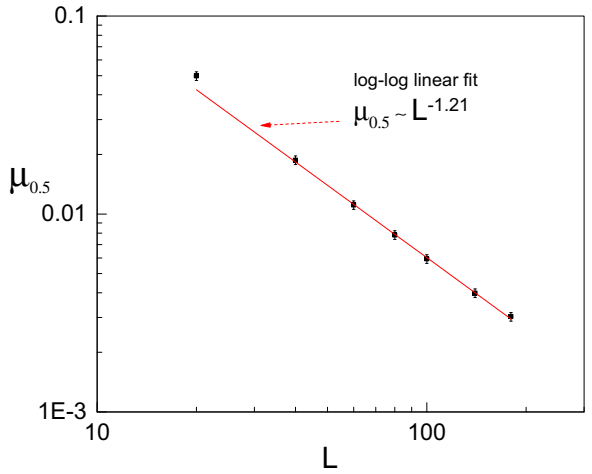

FIG. 11. The log-log plot of the crossover value of $\mu_{0.5}$ vs L taken from the data in Fig. 10.

B. Hysteretic behavior of the smooth-rough dislocation

At temperatures $T < T_H$, the roughening transformation behaves like a first-order phase transition because it shows strong hysteresis (Fig. 12). The width $\Delta\mu$ of the hysteresis (Fig. 13) saturates to a finite value as $T \to 0$ (determined by purely quantum fluctuations). Hysteresis vanishes at $T = T_H \approx 0.0435$ (for the chosen parameters).

We should emphasize that the existence of a phase transition in a 1D system characterized by a local order parameter is forbidden at finite T [27]. In particular, first-order transition should be a crossover characterized by activation with a typical finite energy given by the width of the domain wall between two phases. Thus, the interpretation of the strong hysteresis at finite T requires caution. In this respect we note that, similarly to the dislocation roughening in the presence of the Peierls potential [28], there is no local description of the rough state because it is a global property of the whole dislocation. Thus, the "no-go theorem" [27] does not actually apply. Further studies are required in order to see if the observed hysteresis

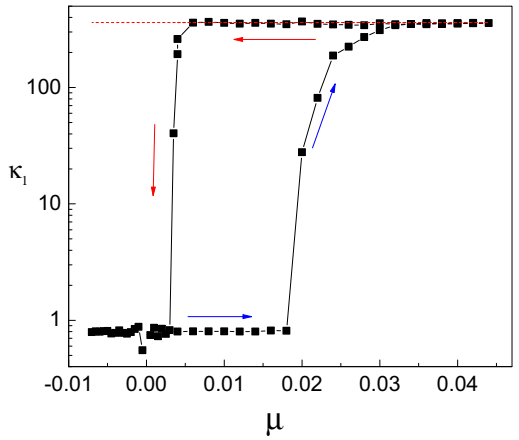

FIG. 12. Hysteretic behavior of the compressibility κ_1 [Eq. (13)] vs μ. The dashed line shows the giant value [Eq. (3)] for $L = 100$, $T = 0.025$, $\rho_0 = 4$, $G = 2.3$. The arrows show the direction of the hysteretic loop: each point corresponds to simulations for 2×10^{10} MC steps for a given value of μ.

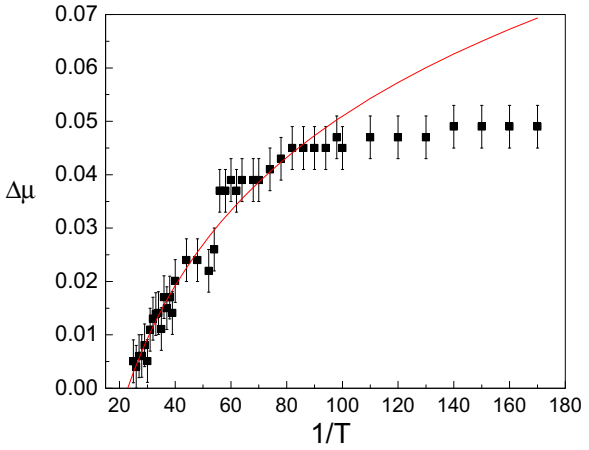

FIG. 13. Width $\Delta\mu$ of the hysteretic loop vs $1/T$ for $L = 100$, $G = 2.3$, $\rho_0 = 4$. Solid line is the fit by $\Delta\mu = \mu_0 \ln(T_H/T)$, $\mu_0 = 0.0346$, $T_H = 0.0436$.

features a true finite-T transition characterized by extensive energy barrier (rather than an intensive one in the case of the crossover).

V. DISCUSSION AND EXPERIMENT PROPOSALS

The effect of emergence of LL behavior in a model which should be a non-LL according to the standard analysis can be viewed from another perspective. The original model (1) features a strong asymmetry between space and time because its excitation spectrum is parabolic: changing unit of space by a factor of 2 requires changing the unit of time by the factor of 4 in order to keep the spectrum unchanged. In the LL phase (smooth phase), the spectrum becomes linear which implies restoration of the space-time symmetry. Furthermore, the nature of the QPT is also consistent with the space-time symmetry. Thus, the edge dislocation with superfluid core features the emergence of the symmetry between space and time (in $D = 1 + 1$) in its ground state in thermodynamic limit.

The question to answer is why the emergence of the LL is not "seen" by the elementary dimensional analysis, and also why there is the BKT transition despite that the KT argument predicts none. The qualitative explanation [29] comes naturally in terms of the loops in Eq. (10). As the weight of each element $\vec{J}$ becomes larger, its discreteness becomes more and more important so that more configurations will have currents J_τ with no neighbors. In such a situation, the discrete gradient $(\nabla_x J_\tau)^2$ becomes essentially J_τ^2. This transforms the action (10) effectively into the form typical for the standard J-current model [23] describing LL as well as the BKT transition at integer filling.

It would be useful to find an argument for the effect in terms of the fields. One insight can be gained from the following consideration: one jog passing along the length L_x of the dislocation carries a string of atoms $\Delta N = L_x$ (which advances an incomplete basal plane by one interatomic distance). This means that each jog is essentially a macroscopically heavy particle as long as $L_x \gg 1$. Thus, such a particle can be localized easily at low T which automatically implies suppression of the superclimb.

Below we will outline proposals for the experiments aimed at testing the most important features of the model. If observed, these would be a proof for the dislocation scenario for the superflow-through-solid and the syringe effects.

A. Stress anisotropy induced by superclimb

The superclimb effect results in injecting (removing) basal atomic planes. For a single hcp crystal confined in a rigid box, this implies additional average deformation along the C axis. If DN atoms were injected to form DM basal layers in a ^{4}He crystal made of M basal layers, the created average strain can be estimated as $u_{zz} \approx DM/M$. This will produce an average stress $\sigma_{zz} \approx C_{zzzz} DM/M$ and $\sigma_{xx} = \sigma_{yy} \approx C_{xxzz} DM/M$, where the z axis is along the hcp axis and x, y are orthogonal coordinates along the basal plane. Here, σ_{ij} is the stress tensor [17] and C_{ijkl} are elastic constants of hcp solid ^{4}He. Thus, the asymmetry of the stress becomes $\alpha_\sigma = \sigma_{zz}/\sigma_{xx} \approx C_{zzzz}/C_{xxzz}$. Measuring the asymmetry and comparing with the known elastic moduli will provide crucial information on the mechanism of the syringe effect. In polycrystals there could also be some asymmetry if the C axis of the crystallites is not fully randomly oriented.

B. Threshold for superclimb

An important aspect of our discussion is the existence of the threshold for superclimb: the syringe effect should vanish in the limits $T \to 0$ and $\mu \to 0$ even in samples free from ^{3}He impurities. (^{3}He suppresses superflow and the syringe [7–9].) At this juncture, it is important to emphasize that stopping the syringe effect does not imply stopping the superflow along the core. Thus, observing a suppression of the syringe effect without suppressing superflow would be a "smoking gun" for the superclimb mechanism [11] and for the emergence of LL. Accordingly, studying the syringe and the superflow effects in extremely clean samples of solid ^{4}He at very low temperatures and biases becomes of crucial importance.

There is, however, a significant obstacle. As mentioned in Ref. [21], the current experiments [7,8] and also [9] are likely to be in the regime of large μ, that is, in the dislocation rough state induced by the bias where $\kappa = \kappa_1 = \kappa_g$ [Eq. (3)], even at $T = 0$. The analysis [21] focuses on the geometrical instability of dislocations with superfluid core: once chemical potential bias exceeds the threshold $\mu_c \sim GL^{-1}$, such dislocations become unstable with respect the inflation which constitutes a mechanism of the crystal growth from inside out. In this case, a single inflating dislocation builds one whole atomic extra plane. As described in Sec. IV A, there is even stronger condition for the destruction of the LL behavior, characterized by the threshold $\mu_c \sim L^{-1.2} \ll L^{-1}$ in the limit $L \to \infty$. Practically, for dislocations with a typical length $L \sim 1$ μm and larger the threshold becomes smaller than $\sim$10 mbar. Translating the temperature scale from Fig. 5, to the temperatures in the units $\sim$1 K, relevant to superfluidity of the dislocations in solid ^{4}He, gives the range $T \leqslant$ 1–10 mK where the suppression of the syringe effect should be looked for. Furthermore, as described in Sec. IV B, there should be strongly hysteretic behavior at low T. Searching for the hysteresis may also provide crucial information. To what extent such measurements at low T and μ are feasible remains to be seen.

C. Equilibrium syringe fraction

As mentioned above, syringe effect implies a liquidlike response of solid on chemical potential. The question is if anything specific can be said about the nature of the conducting network of dislocations. In this respect, an important insight can be gained from Ref. [9]. In this experiment, the upper part of solid ^{4}He (see Fig. 1 of Ref. [9]), which is about 0.3 mm thick, was deformed by about 1 μm. This resulted in an immediate elastic response $\sim$10 mbar at the other end of the sample (about 10 mm away) followed by much slower and stronger pressure increase reaching (equilibrium) values about 0.2 bar [see Fig. 2(a) in Ref. [9]]. It is instructive to compare this number with the pressure imposed in the upper chamber $\sim$0.3–1 bar which resulted from strain $\sim 3 \times 10^{-3}$. Since these values are only a factor of 2–5 different, some information can be drawn about the asymmetry between the lengths of the dislocation network with the help of the relation (6). More consistent studies of the dependence of ΔP vs imposed strain and *in situ* measurements of the compression modulus may shed more light on the nature of the syringe effect.

We also suggest focusing on interaction between glide (see Refs. [17,18]) and superclimb of dislocations as a test for the dislocation scenario. The question is to what extent the giant plasticity of solid ^{4}He [30] may affect the superflow and/or superclimb. The effect [30] consists of softening of the shear modulus G_{el} as temperature increases above $\sim$20–100 mK. While in polycrystalline samples the softening is about 10%–20% of the zero temperature value, in a monocrystal it can reach 80%–90%. The main reason for this effect is glide of basal plane dislocations. It is important to note that these dislocations are not superfluid, and, therefore, they cannot contribute directly to the superclimb. They, however, can affect the syringe response through modifying the shear modulus. We see the main channel for this through contributing to the effective compression modulus K_{el} of the polycrystalline medium as $K_{el} = K_0 + \gamma G_{el}(T)$, with $\gamma > 0$ being a geometrical coefficient determining how averaging of the crystallites orientation contributes to the average K_{el}. Obviously, as G_{el} softens with increasing T, the compression modulus should soften too. In accordance with Eq. (6), this implies a decreasing ΔP with temperature. In this regard we note that, as Fig. 2(a) of Ref. [9] indicates, the equilibrium pressure change is indeed a decreasing function of temperature. More comparative studies of this dependence with the shear softening data [30] will be very useful. [At this point we note that the core tension G of a particular superclimbing segment [see Eqs. (1) and (10)] should not be significantly affected by the plasticity effect in the case of low density of basal dislocations because core of a particular superclimbing edge segment "sees" the ideal crystal in its close vicinity.]

D. Sudden stopping of the pressure evolution

A remarkable feature presented in Fig. 2(a) of Ref. [9] reveals a sudden stopping of the pressure evolution. Clearly, this feature is inconsistent with any type of activation behavior

usually resulting in exponential relaxation. We propose a scenario for this effect: initially long superclimbing dislocations evolve into a structure characterized by small lengths L_x of the free segments. Accordingly, once the resulting chemical potential equilibrates over the whole sample, these segments may enter the LL regime, where the superclimb is suppressed because both μ and T are below the threshold determined by L_x. This should result in the sudden stopping of the pressure variation. More studies of the time evolution can provide crucial information about the nature of this feature.

VI. CONCLUSIONS

We have introduced the J-current type model (10) describing tilted superclimbing dislocation. According to the elementary scaling analysis, such a dislocation should exhibit non-LL behavior. In contrast, Monte Carlo simulations reveal the emergence of the LL as temperature is lowered and the system size exceeds certain scale determined by the line tension G (bare shear modulus). This scale is characterized by high power independent of the bare superfluid stiffness. The emerging LL can also undergo the BKT transition into insulating state. The LL behavior can be destroyed by *macroscopically* small external bias by chemical potential. As a result, the giant isochoric compressibility can be reinstated even at $T = 0$. Our model provides predictions for the corresponding bias and temperature dependencies which can be tested experimentally.

ACKNOWLEDGMENTS

We thank B. Svistunov for fruitful discussions. This work was supported by the NSF Grant No. PHY1314469.

APPENDIX: UNIVERSALITY OF THE TRANSITION TO INSULATING STATE

Here, we support our statement that the quantum transition to the insulating state of the model (9), (10) is of the BKT type. The analysis is conducted for two points at the phase diagram line (Fig. 9), corresponding to $\rho_0 = 0.8, 1$.

The model (9), (10) appears to be very different from the standard J-current model [23] $H_{XY} = \int d^2x\, K(\vec{\nabla}\phi)^2/2$, which describes the compact U(1) phase ϕ in 2D and features the BKT transition at the critical value $K_c = 2/\pi$ of the Luttinger parameter K [19].

If the models (9) and (10) undergo the same type of the transition (at $\mu = 0$), for each value of ρ_0 there should be such a critical value $G = G_c$ that the evolution of the renormalized Luttinger parameter $K = \sqrt{\rho_s \kappa}$ [defined in terms of the windings in Eqs. (11) and (12)] should follow the solution of the renormalization group (RG) equations with the critical value K_c. Such an analysis has been pioneered in Ref. [31].

The RG equations have a form (see Ref. [19])

$$\frac{du}{d\ln l} = 2(1-g)u, \quad \frac{dg^{-1}}{d\ln l} = gu^2\,, \tag{A1}$$

where u stands for the vortex fugacity and $g = K/K_c$. The parameter l determines the typical scale of the renormalization. Numerically, l can be associated with the system size as $l = L/L_0$ up to an arbitrary constant factor L_0.

A general solution of the system (A1) can be expressed in terms of two constants of integration, C, $l_0 > 0$, determined by the initial values of u and g, which in their turn are set by the microscopic model (9), (10). The solution has a form $u^2 = 2[\xi^2 + C]$,

$$F(\xi) = 4\ln\left(\frac{l}{l_0}\right), \quad \xi = \frac{1}{g} - 1 = \frac{K_c}{K} - 1, \tag{A2}$$

where for $C > 0$

$$F(\xi) = \ln[\xi^2(l) + C] - \frac{2}{\sqrt{C}}\tan^{-1}\left(\frac{\sqrt{C}}{\xi}\right) \tag{A3}$$

and

$$F(\xi) = \ln[\xi^2(l) - C^2] + \frac{1}{\sqrt{-C}}\ln\left(\frac{\xi(l) - \sqrt{-C}}{\xi(l) + \sqrt{-C}}\right) \tag{A4}$$

for $C < 0$. The case $C = 0$ describes the separatrix $u = \sqrt{2}|\xi|$ given by

$$F(\xi) = 2\ln|\xi| - \frac{2}{\xi}. \tag{A5}$$

In order to check if the flow of the renormalized Luttinger parameter $K(l)$, obtained from simulations of the model (9), (10) can be described by the RG equations (A1), we tried to fit our Monte Carlo data for K at large L by either solution (A2) or (A4), with the properly chosen C constant for each G. We have analyzed the values $\rho_0 = 0.8, 1.0$ for which the large-L behavior is almost symmetric between space and time. Our finding is that the data can be fit by $C < 0$ [Eq. (A4)] and $\xi > 0$ with $K_c = 2/\pi$ for each value of G.

It is important to note that $C \to 0$ determines a diverging correlation length $L_c \sim \exp(1/4\sqrt{-C}) \to \infty$ with C depending on the deviations from the critical parameter (see Ref. [19]). In our case for fixed ρ_0 we expect $-C \sim G - G_c > 0$ (if the data fit the RG prediction). Practically, the data were substituted into the function F [Eqs. (A2) and (A4)] and plotted vs $4\ln L$. The value of C for a given G has been adjusted so that the slope of F vs $4\ln L$ is unity. A good fit could only be achieved for the solution (A4). The result of this procedure for 10 values of G is presented in Fig. 14. As can

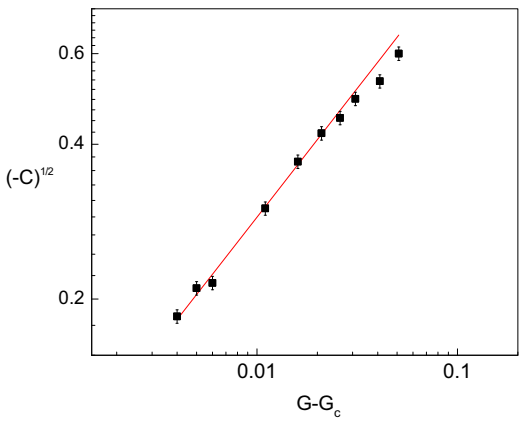

FIG. 14. The parameter $\sqrt{-C}$ versus G for $\rho_0 = 1$. The solid line is the fit by $\sqrt{-C} = A(G - G_c)^{0.5}$, $G_c = 1.299$, $A = 2.886$.

be seen, the data points are consistent with the RG prediction $(-C)^{0.5} \sim (G - G_c)^{0.5}$ with $G_c \approx 1.30$. Thus, the transition is of the BKT type.

The above analysis has been conducted for values ρ_0 and G guaranteeing that the renormalized ρ_s and κ at large $T^{-1} = L$ are approximately equal to each other. This choice was dictated by simplicity of the analysis and also faster convergence of the simulations. It is natural to assume that the universality does not change when ρ_s and κ become significantly asymmetric. Thus, we conclude that the whole line of the transitions $G = G_c(\rho_0)$ in the space ρ_0, G (Fig. 9) belongs to the BKT universality.

[1] P. W. Anderson, Science **177**, 393 (1972); R. B. Laughlin, *A Different Universe (Reinventing Physics from the Bottom Down)* (Basic Books, New York, 2005).

[2] R. B. Laughlin, Rev. Mod. Phys. **71**, 863 (1999).

[3] A. Z. Patashinskii and V. L. Pokrovskii, *Fluctuation Theory of Phase Transitions* (Pergamon, New York, 1979).

[4] F. D. M. Haldane, Phys. Rev. Lett. **47**, 1840 (1981).

[5] T. Giamarchi, *Quantum Physics in One Dimension* (Clarendon, Oxford, 2004).

[6] M. Boninsegni, A. B. Kuklov, L. Pollet, N. V. Prokof'ev, B. V. Svistunov, and M. Troyer, Phys. Rev. Lett. **99**, 035301 (2007).

[7] M. W. Ray and R. B. Hallock, Phys. Rev. Lett. **100**, 235301 (2008); Y. Vekhov and R. B. Hallock, *ibid.* **109**, 045303 (2012); Phys. Rev. B **90**, 134511 (2014).

[8] Z.G. Cheng, J. Beamish, A.D. Fefferman, F. Souris, S. Balibar, and V. Dauvois, Phys. Rev. Lett. **114**, 165301 (2015).

[9] Z. G. Cheng and J. Beamish, Phys. Rev. Lett. **117**, 025301 (2016).

[10] J. Shin, D. Y. Kim, A. Haziot, and M. H. W. Chan, Phys. Rev. Lett. **118**, 235301 (2017).

[11] S. G. Söyler, A. B. Kuklov, L. Pollet, N. V. Prokof'ev, and B. V. Svistunov, Phys. Rev. Lett. **103**, 175301 (2009).

[12] A. B. Kuklov, N. V. Prokof'ev, and B. V. Svistunov, Physics **4**, 109 (2011).

[13] A. F. Andreev and I. M. Lifshitz, Zh. Eksp. Teor. Fiz. **56**, 2057 (1969) [Sov. Phys.–JETP **29**, 1107 (1969)].

[14] M. Boninsegni, A. B. Kuklov, L. Pollet, N. V. Prokof'ev, B. V. Svistunov, and M. Troyer, Phys. Rev. Lett. **97**, 080401 (2006).

[15] L. Pollet, M. Boninsegni, A. B. Kuklov, N. V. Prokof'ev, B. V. Svistunov, and M. Troyer, Phys. Rev. Lett. **101**, 097202 (2008).

[16] L. Pollet, M. Boninsegni, A. B. Kuklov, N. V. Prokof'ev, B. V. Svistunov, and M. Troyer, Phys. Rev. Lett. **98**, 135301 (2007).

[17] L. D. Landau and E. M. Lifshitz, *Theory of Elasticity: Volume 7 (Course of Theoretical Physics)* (Butterworth-Heinemann, Oxford, 1986).

[18] D. Hull and D. J. Bacon, *Introduction to Dislocations* (Butterworth-Heinemann, Oxford, 2007).

[19] T. C. Lubensky, P. M. Chaikin, *Principles of Condensed Matter Physics* (Cambridge University Press, Cambridge, 2000).

[20] A. B. Kuklov, L. Pollet, N. V. Prokof'ev, and B. V. Svistunov, Phys. Rev. B **90**, 184508 (2014).

[21] A. B. Kuklov, Phys. Rev. B **92**, 134504 (2015).

[22] J. Villain, J. Phys. (Paris) **36**, 581 (1975); W. Janke and H. Kleinert, Nucl. Phys. B **270**, 135 (1986).

[23] M. Wallin, E. S. Sörensen, S. M. Girvin, and A. P. Young, Phys. Rev. B **49**, 12115 (1994).

[24] E. L. Pollock and D. M. Ceperley, Phys. Rev. B **36**, 8343 (1987).

[25] N. V. Prokof'ev, B. V. Svistunov, and I. S. Tupitsyn, Phys. Lett. A **238**, 253 (1998); JETP **87**, 310 (1998).

[26] A. M. Polyakov, Gauge Fields and Strings, in *Contemporary Concepts in Physics*, Vol. 3 (Harwood Academic, Chur, 1987), Chap. 4.

[27] L. D. Landau and E. M. Lifshitz, *Statistical Physics, Part I. Volume V (Course of Theoretical Physics)* (Pergamon, Oxford, 1980).

[28] D. Aleinikava and A. B. Kuklov, Phys. Rev. Lett. **106**, 235302 (2011).

[29] B. V. Svistunov (private communication).

[30] A. Haziot, X. Rojas, A. D. Fefferman, J. R. Beamish, and S. Balibar, Phys. Rev. Lett. **110**, 035301 (2013).

[31] N. Prokof'ev and B. Svistunov, Phys. Rev. A **66**, 043608 (2002).